

Multifractal chaotic attractors in a system of delay-differential equations modeling road traffic

Leonid A. Safonov^{a)} and Elad Tomer

Minerva Center and Department of Physics, Bar-Ilan University, 52900 Ramat-Gan, Israel

Vadim V. Strygin

Department of Applied Mathematics and Mechanics, Voronezh State University, 394693 Voronezh, Russia

Yosef Ashkenazy

Center for Global Change Science, Massachusetts Institute of Technology, Cambridge, Massachusetts 02139

Shlomo Havlin

Minerva Center and Department of Physics, Bar-Ilan University, 52900 Ramat-Gan, Israel

(Received 26 December 2001; accepted 25 July 2002; published 13 September 2002)

We study a system of delay-differential equations modeling single-lane road traffic. The cars move in a closed circuit and the system's variables are each car's velocity and the distance to the car ahead. For low and high values of traffic density the system has a stable equilibrium solution, corresponding to the uniform flow. Gradually decreasing the density from high to intermediate values we observe a sequence of supercritical Hopf bifurcations forming multistable limit cycles, corresponding to flow regimes with periodically moving traffic jams. Using an asymptotic technique we find approximately small limit cycles born at Hopf bifurcations and numerically perform their global continuations with decreasing density. For sufficiently large delay the system passes to chaos following the Ruelle–Takens–Newhouse scenario (limit cycles–two-tori–three-tori–chaotic attractors). We find that chaotic and nonchaotic attractors coexist for the same parameter values and that chaotic attractors have a broad multifractal spectrum. © 2002 American Institute of Physics. [DOI: 10.1063/1.1507903]

In many dynamical systems modeled by delay-differential equations (DDEs) the presence of delay can be the reason for chaotic behavior. We consider a system of DDEs which models road traffic. The number of equations in the system is proportional to the number of involved cars and can be arbitrarily high. The nondelay version of the system has a number of limit cycles, corresponding to different jammed flow regimes. For a sufficiently large delay the system exhibits chaotic behavior. We find that different chaotic and nonchaotic attractors coexist for the same parameter values and that chaotic attractors are multifractal.

I. INTRODUCTION

Delay-differential equations have been used to model various natural phenomena including physiological control systems (e.g., Ref. 1), neural networks (e.g., Refs. 2, 3), optical systems (e.g., Refs. 4, 5), chemical reactions (e.g., Refs. 6–8), economic processes (e.g., Ref. 9), mechanical systems (e.g., Ref. 10), road traffic (e.g., Refs. 11, 12), and others. In many studies it was found that time delay can be the reason for chaos in dynamic systems. The presence of delay-induced chaos have been reported in a number systems of delay-differential equations, which are mostly of low order.

In this paper we study the transition to chaos in a system

of DDEs which models road traffic. The order of the system can be arbitrarily high depending on the number of cars and is taken to be equal to 200.

The presence of chaotic phenomena in traffic models has been reported before. Addison and Low¹² observed chaos in a car-following model in which the leading car has an oscillating velocity. Nagatani¹³ described the chaotic jam phase in a lattice hydrodynamic model derived from the optimal velocity model.¹⁴

Unlike these studies, our model is based on a high-order system of autonomous delay-differential equations and chaotic effects are observed only for sufficiently large delay.

We find that the system passes to chaos according to the following scenario: stable steady state–multistable limit cycles–two-tori–three-tori–chaotic attractors, which is known as the Ruelle–Takens–Newhouse route to chaos.¹⁵ This scenario was observed, for example, for the first order Ikeda delay-differential equation,⁴ where the coexistence of chaotic attractors was also reported. Transition to chaos from two-tori was also found in other models of different natural phenomena based on delay equations, for example, by tori doubling sequence,¹⁰ and other routes.^{16–18}

We generalize the model proposed and studied in Refs. 19–21 by introducing time delay in the driver's reaction. The model is based on the assumption that N cars move a single lane (Fig. 1) and the n th car motion is described by the delay-differential equation,

^{a)}Author to whom correspondence should be addressed. Electronic mail: leonid@ory.ph.biu.ac.il

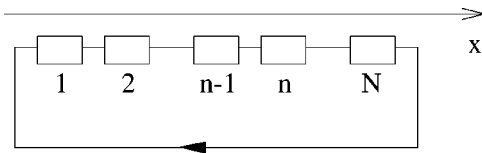


FIG. 1. Scheme of the model.

$$\frac{d^2x_n(t)}{dt^2} = A \left(1 - \frac{\Delta x_n^0(t-\tau)}{\Delta x_n(t-\tau)} \right) - \frac{Z^2(-\Delta v_n(t-\tau))}{2(\Delta x_n(t-\tau) - D)} - kZ(v_n(t-\tau) - v_{per}), \tag{1}$$

where $n = 1, \dots, N$, x_n is the car's coordinate, v_n is its velocity, A and k are the sensitivity parameters, D , is the minimal distance between consecutive cars, v_{per} is the permitted velocity, T is the safety time gap, $\Delta x_n^0 = v_n T + D$ is the safety distance, $\Delta x_n = x_{n+1} - x_n$, $\Delta v_n = v_{n+1} - v_n$, and τ is the time delay. $Z(x) = x\Theta(x)$ (Θ is the Heaviside step function). As in Refs. 19–21 we use the parameters values $v_{per} = 25$ (m/s), $T = 2$ (s), $D = 5$ (m), $A = 3$ (m/s²), and $k = 2$ (s⁻¹). We assume that $N = 100$ and that the boundary conditions are periodic, i.e., $x_{N+1} = x_1 + L$, $v_{N+1} = v_1$, where L is the road length.

The first term in Eq. (1) is dominant when the velocity difference between consecutive cars is relatively small. In this case the n th car accelerates if $\Delta x_n > \Delta x_n^0$ and brakes if $\Delta x_n < \Delta x_n^0$. The second term plays an important role when $v_n \gg v_{n+1}$. A car getting too close to a much slower car starts braking even before getting within the safety distance $\Delta x_n > \Delta x_n^0$. This term corresponds to the negative acceleration needed to reduce $|\Delta v_n|$ to 0 as $\Delta x_n \rightarrow D$. The dissipative third term is a repulsive force acting when the velocity exceeds the permitted velocity.

Nonlinear phenomena in the nondelay version of the model were extensively studied in Ref. 21. It was found that system (1) with $\tau = 0$ in variables $(\Delta x_n, v_n)$ has many stable limit cycles. Any such cycle corresponds to a flow regime in which all cars in the circuit are grouped into a number of equidistant moving dense regions (jams). Each cycle is uniquely characterized by the total number of these regions. It was found²¹ that limit cycles emerge at Hopf bifurcations with ρ decreasing from high to intermediate values. For densities close to bifurcation values the cycles were found analytically and traced numerically with a further decrease of density.

In this paper we present the generalization of the model for the time delay case. Applying an approach similar to that of Ref. 21 to the study of the Hopf bifurcation in delay-differential equations we find that for sufficiently large delay the system can behave in a complicated manner. Solving system (1) numerically and performing the power spectrum analysis of the resulting time series, we show that periodic solutions described above may bifurcate into two-tori, which subsequently bifurcate into three-tori, which are later destroyed forming chaotic attractors. We also measure the generalized correlation dimension of a reconstructed chaotic attractor and find that this attractor is multifractal.

The paper is organized as follows: In Sec. II we perform a linear stability analysis and in Sec. III find approximately small limit cycles born at Hopf bifurcations. Section IV is devoted to global continuation of the cycles, study of their bifurcations into two- and three-tori, transition to chaos, and the analysis of properties of chaotic attractors. A summary is given in Sec. V.

II. LINEAR STABILITY ANALYSIS

Hopf bifurcation in delay-differential equations is a well understood phenomenon. Many numerical techniques for analysis of Hopf bifurcations have been developed, the three most widely used being the integral averaging,²² the Lyapunov–Schmidt reduction,²³ and the Poincaré normal form.^{16,24,25} These techniques are also applicable to multiple Hopf bifurcations, where many pairs of complex eigenvalues gain positive real parts. The former two allow one to find first approximations of small periodic solutions emerging at a Hopf bifurcation. The technique described below is based on a method proposed in Ref. 26 for ordinary differential equations and used in Ref. 21 for the analysis of the nondelay version of our model. Although it allows us to find higher order approximations of the small limit cycle we find only the first approximation and use it for further numerical analysis.

System (1) has the following solution:

$$v_n^0 = v^0 = \begin{cases} \frac{A(1-D\rho) + kv_{per}}{A\rho T + k}, & \rho \leq \frac{1}{D + Tv_{per}}, \\ \frac{1-D\rho}{\rho T}, & \rho > \frac{1}{D + Tv_{per}}, \end{cases} \tag{2}$$

$$x_n^0 = \frac{n-1}{\rho} + v^0 t,$$

where $\rho = N/L$ is the flow density. This solution corresponds to the homogeneous flow, in which all cars have the same velocity, and spaces between neighboring cars are all equal.

We introduce a new variable

$$\xi_n = \Delta x_n - 1/\rho$$

in Eq. (1). This change of variables maps the homogeneous flow solution (2) to zero. Its stability can be analyzed using the linearization of Eq. (1),

$$\ddot{\xi}_n^0(t) = -p\xi_n^0(t-\tau) + q(\xi_{n+1}^0(t-\tau) - \xi_n^0(t-\tau)), \tag{3}$$

where

$$p = AT\rho + k, q = \frac{AT + kTv_{per} + kD}{AT\rho + k} \cdot A\rho^2$$

$$\text{if } \rho \leq \frac{1}{D + Tv_{per}},$$

and $p = AT\rho$, $q = A\rho$ otherwise.

Following Refs. 14, 19, we look for a solution of Eq. (3) in the form,

$$\xi_n^0 = \exp(i\alpha_\kappa n + \lambda t), \tag{4}$$

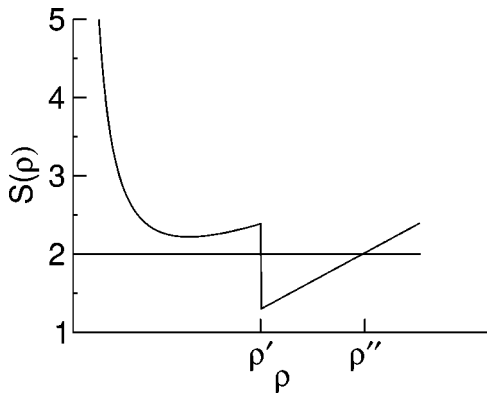


FIG. 2. Schematic plot of function $S(\rho)$. $\rho' = 1/(D + Tv_{per})$, $\rho'' = 2/AT^2$.

where $\alpha_\kappa = (2\pi/N)\kappa$ ($\kappa = 0, \dots, N-1$) and λ is a complex number. Substituting (4) into Eq. (3) we obtain the equation for λ ,

$$\lambda^2 + [p\lambda - q(e^{i\alpha_\kappa} - 1)]e^{-\lambda\tau} = 0. \tag{5}$$

The solutions of N equations (5) are the eigenvalues of system (3). One of these solutions (for $\kappa = 0$) is zero. Other solutions are negative for sufficiently high and sufficiently low values of ρ , which indicates the stability of the homogeneous flow solution.

For the nondelay version of the model the stability condition was found¹⁹ to be $S(\rho) = \rho^2/q > 2$, where

$$S(\rho) = \begin{cases} \frac{(AT\rho + k)^3}{\rho^2 A(AT + kv_{per}T + kD)}, & \rho \leq \frac{1}{D + Tv_{per}}, \\ A\rho T^2, & \rho \geq \frac{1}{D + Tv_{per}}. \end{cases}$$

The function $S(\rho)$ is plotted in Fig. 2. Its discontinuity [which is a consequence of discontinuity of $p(\rho)$ and $q(\rho)$]

is conditioned by the fact that the right-hand side of (1) is not continuously differentiable.²⁷ With small delay this stability condition does not change qualitatively.

As ρ increases from low values (decreases from high values) pairs of complex solutions of Eq. (5) cross the imaginary axis causing the formation of small periodic solutions (Hopf bifurcations). We observe that due to the discontinuity of $p(\rho)$ and $q(\rho)$ for low density values, the loss of stability occurs abruptly with real parts of many pairs of complex eigenvalues becoming positive together. But for high densities (and, respectively, low velocities) the last term in the right-hand side of Eq. (1) is zero and functions $p(\rho)$ and $q(\rho)$ are continuous. Our numerical analysis shows that some pairs of complex eigenvalues cross the imaginary axis consecutively as the density changes from high to intermediate values. We also find that cycles born at these Hopf bifurcations are stable, i.e., the bifurcations are supercritical.

III. HOPF BIFURCATIONS, APPROXIMATE FINDING OF SMALL LIMIT CYCLES

This section is devoted to the analytical approximation of these periodic solutions for density values close to high bifurcation values. For the study of bifurcations we propose the following approach. Let Eq. (1) be written as

$$\frac{dx}{dt} = f(x(t), x(t - \tau), \rho), \tag{6}$$

where $x = (\xi_1, w_1, \xi_2, w_2, \dots, \xi_N, w_N)^T \in \mathbf{R}^{2N}$ and $w_n = v_n - v_0$. The zero solution of (6) corresponds to the homogeneous flow solution (2).

We can rewrite (6) as

$$\begin{aligned} \frac{dx}{dt} = & M_1 x(t) + M_2(\rho) x(t - \tau) + f_2(x(t), x(t - \tau), \rho) \\ & + \mathcal{R}(x(t), x(t - \tau), \rho), \end{aligned} \tag{7}$$

where

$$M_1 = \begin{pmatrix} 0 & -1 & 0 & 1 & 0 & 0 & \dots & 0 & 0 \\ 0 & 0 & 0 & 0 & 0 & 0 & \dots & 0 & 0 \\ 0 & 0 & 0 & -1 & 0 & 1 & \dots & 0 & 0 \\ 0 & 0 & 0 & 0 & 0 & 0 & \dots & 0 & 0 \\ \cdot & \cdot \\ 0 & 1 & 0 & 0 & 0 & 0 & \dots & 0 & -1 \\ 0 & 0 & 0 & 0 & 0 & 0 & \dots & 0 & 0 \end{pmatrix},$$

$$M_2(\rho) = \begin{pmatrix} 0 & 0 & 0 & 0 & 0 & 0 & \dots & 0 & 0 \\ q(\rho) & -p(\rho) & 0 & 0 & 0 & 0 & \dots & 0 & 0 \\ 0 & 0 & 0 & 0 & 0 & 0 & \dots & 0 & 0 \\ 0 & 0 & q(\rho) & -p(\rho) & 0 & 0 & \dots & 0 & 0 \\ \cdot & \cdot \\ 0 & 0 & 0 & 0 & 0 & 0 & \dots & 0 & 0 \\ 0 & 0 & 0 & 0 & 0 & 0 & \dots & q(\rho) & -p(\rho) \end{pmatrix}$$

is the linearization of (6) near zero, $f_2(x, \rho)$ are the second order terms and $\mathcal{R}(x, \rho)$ are the higher order terms.

It is known²⁸ that equation

$$\frac{dx}{dt} = M_1 x(t) + M_2 x(t - \tau) \tag{8}$$

defines a strongly continuous semigroup in the space of continuous $[-\tau, 0] \rightarrow \mathbf{R}^{2N}$ functions. As \mathcal{A} we denote the infinitesimal generator of this semigroup.

If λ is an eigenvalue of \mathcal{A} found from (5), then the corresponding eigenfunction defined on $[-\tau, 0]$ can be found as

$$g(\lambda, t) = e^{-\lambda t} \left(e^{i\alpha_\kappa}, \frac{qe^{i\alpha_\kappa - \lambda\tau}}{\lambda + pe^{-\lambda\tau}}, e^{2i\alpha_\kappa}, \frac{qe^{2i\alpha_\kappa - \lambda\tau}}{\lambda + pe^{-\lambda\tau}}, \dots, e^{(N-1)i\alpha_\kappa}, \frac{qe^{(N-1)i\alpha_\kappa - \lambda\tau}}{\lambda + pe^{-\lambda\tau}}, 1, \frac{qe^{-\lambda\tau}}{\lambda + pe^{-\lambda\tau}} \right)^T.$$

The system conjugate to (8) (Ref. 28) has the form,

$$\frac{dx}{dt} = -M_1^T x(t) - M_2^T x(t + \tau). \tag{9}$$

Its eigenfunction corresponding to the eigenvalue λ is

$$h(\lambda, t) = e^{\lambda t} \left(-\frac{qe^{i\alpha_\kappa + \lambda\tau}}{\lambda}, e^{i\alpha_\kappa}, -\frac{qe^{2i\alpha_\kappa + \lambda\tau}}{\lambda}, e^{2i\alpha_\kappa}, \dots, -\frac{qe^{(N-1)i\alpha_\kappa + \lambda\tau}}{\lambda}, e^{(N-1)i\alpha_\kappa}, -\frac{qe^{\lambda\tau}}{\lambda}, 1 \right)^T$$

for $\lambda \neq 0$.

Let for $\rho = \rho_0$ the generator \mathcal{A} have a pair of imaginary eigenvalues $\pm i\omega$. Then Eq. (8) has two $2\pi/\omega$ -periodic linearly independent solutions $\varphi_1(t) = \text{Re } g(i\omega, t)$ and $\varphi_2(t) = \text{Im } g(i\omega, t)$. Similarly, Eq. (9) has two $2\pi/\omega$ -periodic linearly independent solutions $\psi_1(t)$ and $\psi_2(t)$, defined by $h(i\omega, t)$. Without loss of generality we can assume that

$$\frac{\omega}{2\pi} \int_0^{2\pi/\omega} \langle \varphi_i(t), \psi_j(t) \rangle dt = \delta_{ij},$$

where $i, j = 1, 2$, δ_{ij} is the Kronecker symbol and $\langle \cdot, \cdot \rangle$ denotes the scalar product in \mathbf{R}^{2N} .

Let $\rho = \rho_0 - \varepsilon$. Then $M_2(\rho) = M_2(\rho_0 - \varepsilon) = M_2^0 - \varepsilon B_2 + O(\varepsilon^2)$, where $M_2^0 = M_2(\rho_0)$ and $B = \partial M_2(\rho_0) / \partial \rho$. System (7) can be rewritten as

$$\begin{aligned} \frac{dx}{dt} &= M_1 x(t) + M_2^0 x(t - \tau) - \varepsilon B x(t - \tau) \\ &\quad + f_2(x(t - \tau), \rho_0 - \varepsilon) + O((\|x\| + |\varepsilon|)^3). \end{aligned} \tag{10}$$

In order to find a small cycle we replace ε in (10) with a new small parameter c , such that²⁶

$$\varepsilon = c\gamma_1 + c^2\gamma_2 + \dots \tag{11}$$

and introduce a new time s in the form,

$$s = t / (1 + c\mu_1 + c^2\mu_2 + \dots), \tag{12}$$

where $\gamma_1, \gamma_2, \dots$ and μ_1, μ_2, \dots are yet unknown parameters.

We are looking for a small limit cycle of the system (10) in the form

$$x^*(t) = y^*(s) = cy_1(s) + c^2y_2(s) + \dots, \tag{13}$$

where y_1, y_2, \dots are unknown $2\pi/\omega$ -periodic functions of s .

Substituting (11)–(13) into Eq. (10) and equating the terms with the same powers of c we obtain that $y_1(s)$ is a $2\pi/\omega$ -periodic solution of (8). We can assign $y_1(s) \equiv \varphi_1(s)$.

Obviously, $y_2(s)$ can be found as a $2\pi/\omega$ -periodic solution of

$$\begin{aligned} \frac{dy_2}{ds} &= M_1 y_2(s) + M_2^0 y_2(s - \tau) \\ &\quad + \mathcal{F}_2(\varphi_1(s), \varphi_1(s - \tau), \mu_1, \gamma_1), \end{aligned} \tag{14}$$

where

$$\begin{aligned} \mathcal{F}_2 &= \mu_1 M_1 \varphi_1(s) + \mu_1 M_2^0 \varphi_1(s - \tau) \\ &\quad + \tau \mu_1 M_2^0 \varphi_1'(s - \tau) - \gamma_1 B_2 \varphi_1(s - \tau) \\ &\quad + f_2(\varphi_1(s - \tau), \rho_0). \end{aligned}$$

As shown in Ref. 29, for system (14) to have a periodic solution it is necessary and sufficient that

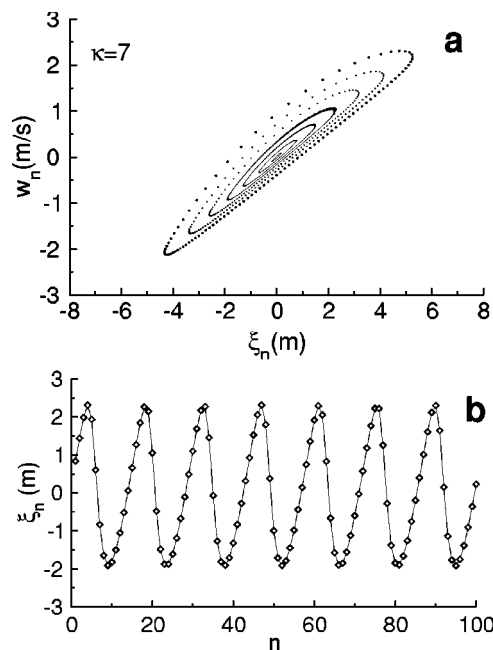


FIG. 3. Global continuation of the cycle with $\kappa = 7$ for $\tau = 0$. (a) w_n versus ξ_n (each dot corresponds to a car). The innermost loop corresponds to the analytically found small cycle near the Hopf bifurcation point $\rho \approx 0.159$. The others represent the numerical continuation of the cycle with the step $\Delta\rho = -0.01$. (b) ξ_n versus n [ρ is the same as for the last step of (a)].

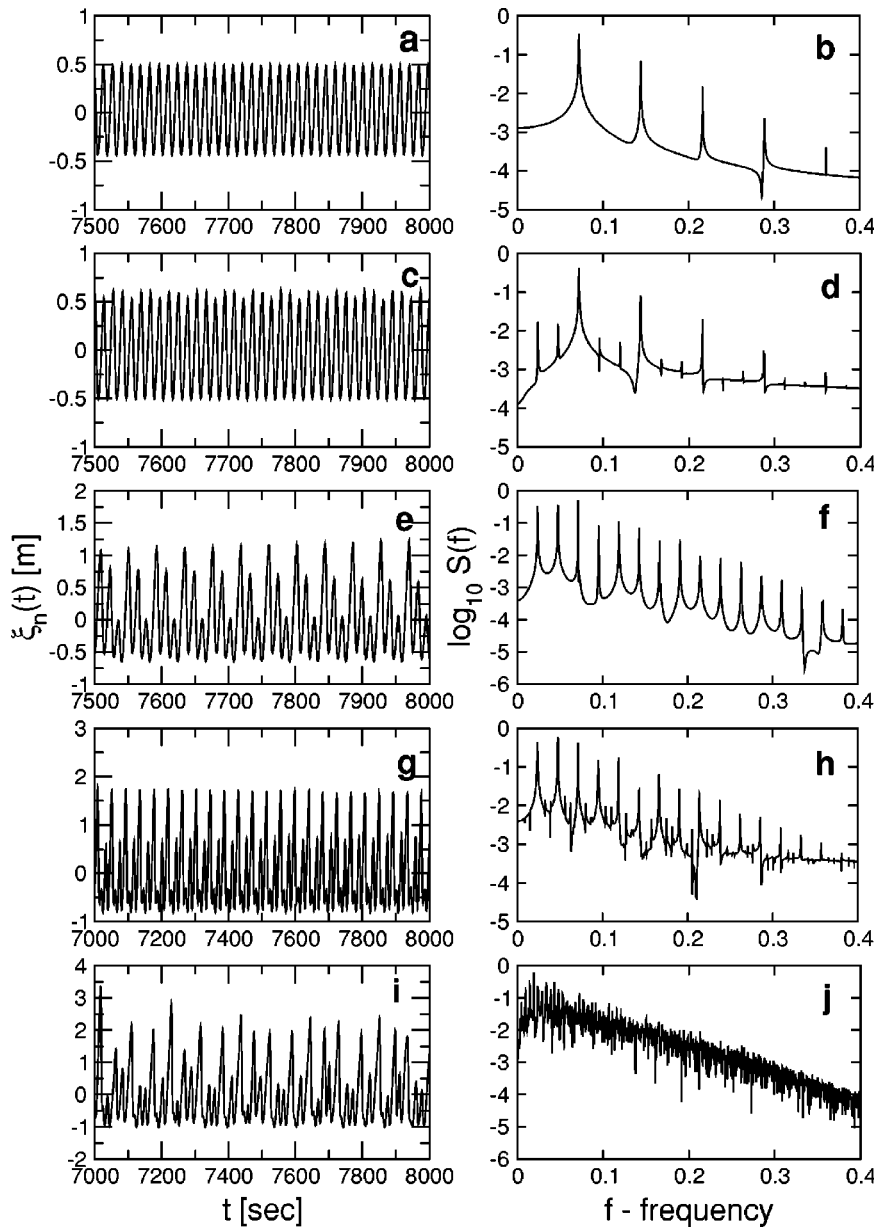


FIG. 4. Transition to chaos from the periodic solution with $\kappa=15$. $N=100$, $\tau=0.59$. Left column, dependence of $\xi_n(t)$ for $n=10$; right column, corresponding power spectra. (a), (b) $\rho=0.1492$; (c), (d) $\rho=0.1467$; (e), (f) $\rho=0.1442$; (g), (h) $\rho=0.1402$; (i), (j) $\rho=0.1387$.

$$\int_0^{2\pi/\omega} \langle \mathcal{F}_2(\varphi_1(s), \varphi_1(s-\tau), \mu_1, \gamma_1), \psi_i(s) \rangle ds = 0$$

for $i=1,2$. This condition yields two equations with unknown μ_1 and γ_1 . Therefore the first approximation of the periodic solution of (10) is found as

$$x^*(t) = \frac{\varepsilon}{\gamma_1} \varphi_1(t). \tag{15}$$

This solution has the period $T = (2\pi/\omega)(1 + \mu_1(\varepsilon/\gamma_1)) + O(\varepsilon^2)$. Higher approximations of the solution can be found using the described above algorithm. Note that according to (4) there exists an integer $1 \leq \kappa \leq N-1$ such that the flow state corresponding to solution (15) is a wave with the wavelength L/κ (in length units) or N/κ (in number of cars).

IV. GLOBAL CONTINUATION OF LIMIT CYCLES, TRANSITION TO CHAOS

After the small limit cycle for density close to the Hopf bifurcation value is found analytically, its global continuation is performed numerically in the following manner. For $\rho \approx \rho_0 - \varepsilon$ we take the analytically found approximate periodic solution as an initial condition and solve Eq. (1) numerically. After the solution has reached an attracting set, we decrease ρ with a small step and solve the equations numerically again, taking the results from the previous step as initial conditions. This procedure is iterated further. In this way we keep the track of the particular limit cycle. Results of the first stages of an execution of this algorithm are presented in Fig. 3.

For the nondelay case we have not found any other attracting sets than fixed points and limit cycles. With a small

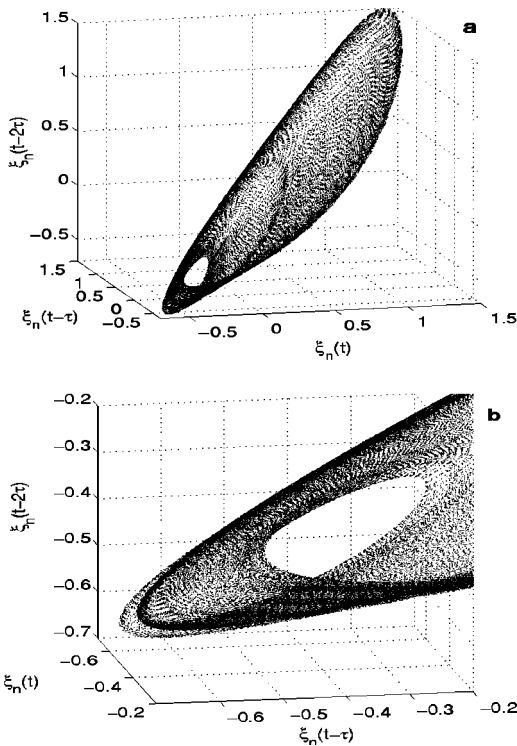


FIG. 5. (a) Time delay reconstruction of a two-torus. Parameters are the same as in Figs. 4(e) and 4(f). (b) Magnification of a part of (a).

delay the system's behavior does not change qualitatively. For higher values of τ the cycles may undergo bifurcations leading to transition to chaos.

Figure 4 illustrates the transition to chaos from the cycle with $\kappa=15$ for $\tau=0.59$ and $N=100$. The cycle was formed

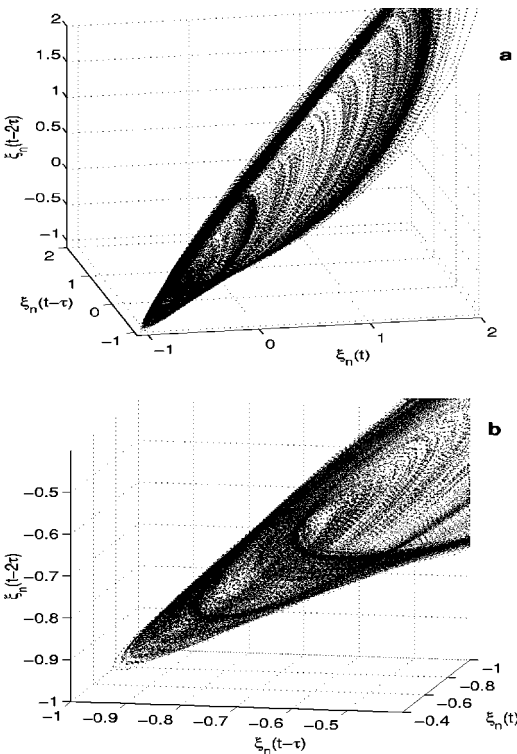


FIG. 6. (a) Time delay reconstruction of a chaotic attractor. Parameters are the same as in Figs. 4(i) and 4(j). (b) Magnification of a part of (a).

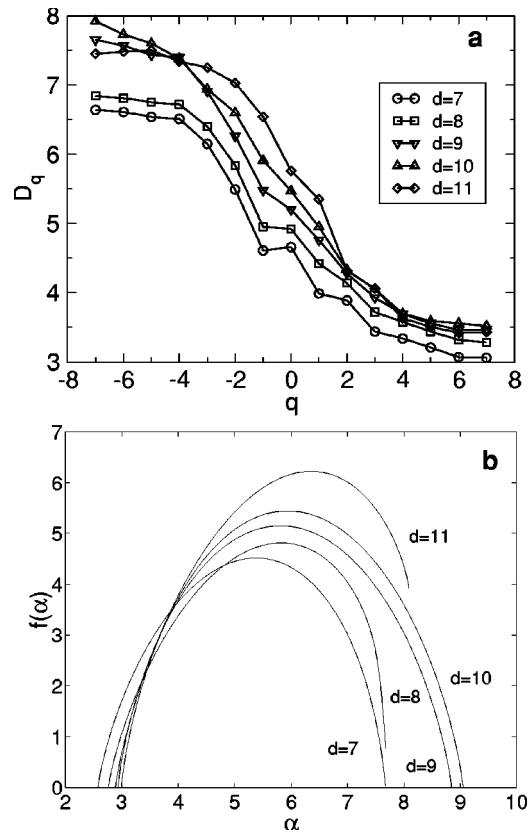


FIG. 7. (a) Results of measurement of the correlation dimension D_q for moments $q = -7 \dots 7$ and embedding dimensions $d = 7 \dots 11$ (bottom to top). The parameter values are the same as in Figs. 4(i) and 4(j). (b) Approximate $f(\alpha)$ fits for these data.

after a Hopf bifurcation at $\rho \approx 0.1665$. Figures 4(a), 4(c), 4(e), 4(g), and 4(i) show the dependence of ξ_n for an arbitrarily chosen n on t for different values of ρ . Presented in Figs. 4(b), 4(d), 4(f), 4(h), and 4(j) are the corresponding power spectra. Figures 4(a) and 4(b) present the fully developed limit cycle. Figures 4(c) and 4(d) depict the loss of stability by this cycle at $\rho \approx 0.1467$. It can be seen from Fig. 4(d) that a new independent frequency which is approximately three times smaller than the original one appears. This indicates a bifurcation of a two-torus from the cycle. The system's motion on the torus is quasiperiodic, which is illustrated in Figs. 4(e) and 4(f). A three-dimensional time-delay reconstruction of the two-torus for $\kappa=15$ is shown in Fig. 5.

As we continue to decrease ρ further we find that at $\rho \approx 0.1402$ one more independent frequency emerges, which is nearly three times smaller than the previous one. This is an indication of a bifurcation of a three-torus from the two-torus. The motion on the three-torus is illustrated in Figs. 4(g) and 4(h). This three-frequency quasiperiodic motion is observed only over a limited time interval, after which it becomes more complex. This indicates that the system is driven to chaos by a small computational error according to the Ruelle–Takens theory.¹⁵

With further decrease of density the motion becomes chaotic. The fully developed chaotic regime is shown in Figs. 4(i) and 4(j) and a three-dimensional time-delay recon-

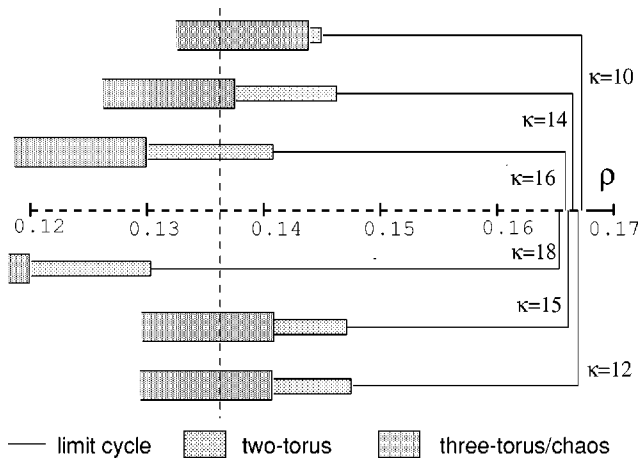


FIG. 8. A schematic bifurcation diagram, showing transition to chaos from six different limit cycles for $\tau=0.59$. The figure shows that limit cycles, two-tori, and chaotic attractors can coexist for the same parameter values (see the vertical dashed line).

struction of the chaotic attractor is presented in Fig. 6. Since, as shown below, the attractor's dimension is >3 , the fragment of the trajectory used here is taken short enough not to fill a three-dimensional volume. The exponential decay of the power spectrum in Fig. 4(j) is an additional sign of chaotic behavior of our system. This decay can be associated with the sharp decrease of the autocorrelation function at large scale, which is characteristic to chaos.³⁰

The most widely used characteristic of multifractality of a chaotic set is the $f(\alpha)$ function which represents the spectrum of fractal dimensions.³¹

To fit this function approximately we use the so-called method of moments.³² The method is based on measuring the

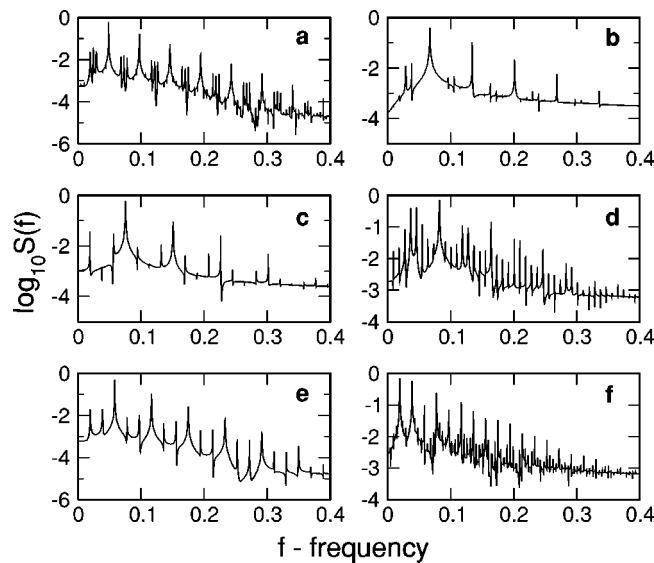


FIG. 9. (a)–(e). Power spectra of the solutions originated from limit cycles with $\kappa=10$ ($\rho=0.1449$), $\kappa=14$ ($\rho=0.1459$), $\kappa=16$ ($\rho=0.1410$), $\kappa=18$ ($\rho=0.1303$), and $\kappa=12$ ($\rho=0.1476$), respectively, immediately after the limit cycle \rightarrow two-torus bifurcation. The ratio of the new frequency to the old one is close to a divisor of κ (10, 7, 4, 9, and 3, respectively). (f) Power spectrum of the solution originated from the cycle with $\kappa=12$ ($\rho=0.1420$) after the two-torus \rightarrow three-torus bifurcation. The frequencies ratio is also close to an integer.

generalized correlation dimension³³ of the attractor. To measure the correlation dimension we reconstruct the attractor from a single car time series $\xi_n(t)$, taking consecutive d -tuples of values $\mathbf{x}_i=(\xi_n(t_i), \xi_n(t_i+\Delta t), \dots, \xi_n(t_i+(d-1)\Delta t))$ as d -dimensional phase vectors (d is called embedding dimension³³ and Δt is the the first zero of the time series autocorrelation function).

We consider the correlation function of the moment q ,

$$C_q(r) = \left[\frac{1}{M} \sum_{i=1}^M \left[\frac{1}{M} \sum_{j=1}^M \Theta(r - |\mathbf{x}_i - \mathbf{x}_j|) \right]^{q-1} \right]^{1/(q-1)},$$

where Θ is the Heaviside step function and M is the time series length, which should be sufficiently large. The correlation dimension D_q is defined by the relation $C_q(r) \sim r^{D_q}$ (see Refs. 33, 34, and references therein for more details). To find the correlation dimensions numerically we use the algorithm proposed in Ref. 34.

Figure 7(a) shows the results of measurements of D_q for $q=-7 \cdot \cdot 7$ and $d=7 \cdot \cdot 11$. Fitting these data with a continuous function $D(q)$ for each d , we find the $f(\alpha)$ function according to the formula

$$f(\alpha(q)) = q\alpha(q) - \tau(q),$$

where $\tau(q) = (q-1)D(q)$ and $\alpha(q) = d\tau(q)/dq$ (see, e.g., Ref. 31).

As can be observed from Fig. 7(a), the values of D_q show weak convergence with growing q , especially for d close to 0. Therefore, presented values of dimensions may be underestimated. Nevertheless, the broadness of the $f(\alpha)$

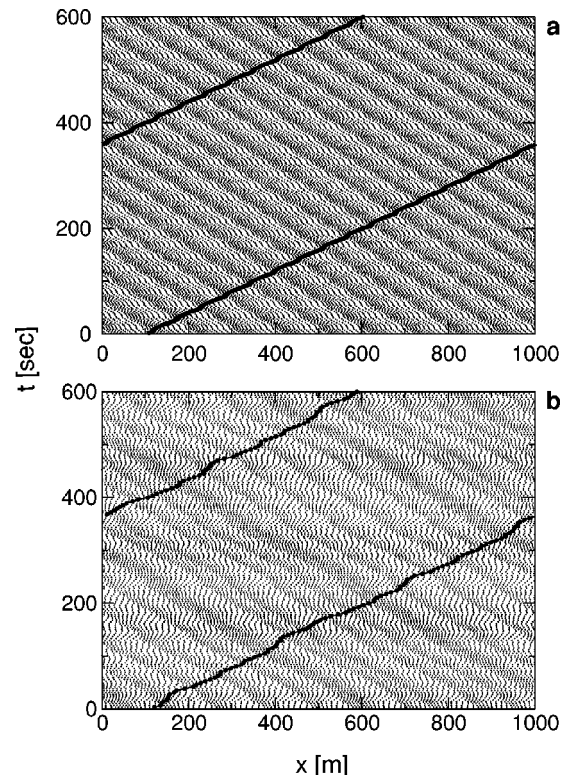


FIG. 10. Space–time diagrams of the traffic flow for $\kappa=10$ and $\rho=0.1$. (a) $\tau=0.4$ (a limit cycle); (b) $\tau=0.59$ (chaos). Each dot corresponds to a car. Bold dots represent the trajectory of a single car.

curves for each d (especially for $q \leq 0$) enables us to claim the multifractality of the considered attractor.

The chaoticity of the attractor can also be characterized by the existence of positive Lyapunov exponents. The Kaplan–Yorke conjecture connects the Lyapunov dimension D_L with the Lyapunov exponents spectrum by

$$D_L = j + \sum_{i=1}^j \lambda_i / |\lambda_{j+1}|,$$

where the Lyapunov exponents are sorted in decreasing order ($\lambda_1 > \lambda_2 > \dots > \lambda_n$) and j is defined by the conditions $\sum_{i=1}^j \lambda_i > 0$ and $\sum_{i=1}^{j+1} \lambda_i < 0$. Since $D_L \geq D_2$,³⁵ our system has at least one positive Lyapunov exponent. A direct calculation of the largest Lyapunov exponent³⁶ and the Lyapunov exponents spectrum³⁷ yields three positive Lyapunov exponents of order 10^{-4} . Because these exponents are small and close to each other, they cannot be used to accurately estimate D_L .

We perform similar studies of transition to chaos from several other cycles (with different κ). Figure 8 is a schematic bifurcation diagram showing that the bifurcations of the same type occur at different density values for different cycles. It also shows that attractors of different types (including chaotic and nonchaotic ones) coexist for the same parameter values.

Another important observation is that the ratio of the old frequency to the new one at the limit cycle \rightarrow torus bifurcation is close to a divisor of the corresponding κ . For example, it is close to 10 for $\kappa = 10$ [Fig. 9(a)], 7 for $\kappa = 14$ [Fig. 9(b)], 4 for $\kappa = 16$ [Fig. 9(c)], 9 for $\kappa = 18$ [Fig. 9(d)], and 3 for $\kappa = 12$ [Fig. 9(e)]. At the two-torus \rightarrow three-torus bifurcation the ratio between the new and the previous frequency is also close to an integer, which is different for different tori. For example, Fig. 9(f) shows that for $\kappa = 12$ this ratio is close to 4, while for $\kappa = 15$ it is nearly 3 [Fig. 4(h)].

Figure 10 demonstrates how the introduction of delay into the model equations affects the traffic flow generated by the model. Presented on the figure are space–time diagrams for a periodic and a chaotic regimes. Obviously, in the latter case the flow is more complex. It is well known that complexity of real traffic is due to various heterogeneities (of driver behaviors, vehicles, the road, etc.). Our model, despite not taking all these factors into account, is, nevertheless, able to demonstrate irregular behavior attributed only to the delay in the driver's reaction.

V. SUMMARY

A model of single-lane road traffic based on a system of delay-differential equations is studied. It is found that the presence of time delay accounts for the chaotic behavior of the system. The transition to chaos is found to follow the Ruelle–Takens–Newhouse scenario, which is stable steady state–two-dimensional tori–three-dimensional tori–chaotic attractors. The motion on the tori is periodic or quasiperiodic and many different tori and chaotic attractors coexist for the same parameter values. We also find that chaotic attractors have multifractal properties.

ACKNOWLEDGMENTS

We would like to thank I. Dana for useful comments. One of us (Y.A.) thanks the Bikura fellowship for partial support.

- ¹M. C. Mackey and L. Glass, "Oscillation and chaos in physiological control systems," *Science* **197**, 287–289 (1977); A. Beuter, J. G. Milton, C. Labrie, L. Glass, and S. Gauthier, "Delayed visual feedback and movement control in Parkinson's disease," *Exp. Nephrol.* **110**, 228–235 (1990).
- ²J. Bélair, S. A. Campbell, and P. van der Driessche, "Frustration, stability, and delay-induced oscillations in a neural network model," *SIAM (Soc. Ind. Appl. Math.) J. Appl. Math.* **56**, 245–255 (1996).
- ³C. M. Markus, F. R. Waugh, and R. M. Westervelt, "Nonlinear dynamics and stability of analog neural networks," *Physica D* **51**, 234–247 (1991).
- ⁴K. Ikeda and K. Matsumoto, "High-dimensional chaotic behavior in systems with time-delayed feedback," *Physica D* **29**, 223–235 (1987).
- ⁵C. Hager and F. Kaiser, "Bifurcation structures into chaos of delay-differential equations for a passive optical ring resonator," *Appl. Phys. B: Photophys. Laser Chem.* **55**, 132–137 (1992).
- ⁶J. Weiner, F. W. Schneider, and K. Bar-Eli, "Delayed-output-controlled chemical oscillations," *J. Phys. Chem.* **93**, 2704–2711 (1989).
- ⁷T. Chevalier, A. Freund, and J. Ross, "The effects of a nonlinear delayed feedback on a chemical reaction," *J. Chem. Phys.* **95**, 308–316 (1991).
- ⁸K. Bareli and R. M. Noyes, "Gas-evolution oscillators. 10. A model based on a delay equation," *J. Phys. Chem.* **96**, 7664–7670 (1992).
- ⁹M. Mackey, "Commodity price fluctuations: Price dependent delays and nonlinearities as explanatory factors," *J. Econ. Theory* **48**, 497–509 (1989).
- ¹⁰M. A. Johnson and F. C. Moon, "Experimental characterization of quasi-periodicity and chaos in a mechanical system with delay," *Int. J. Bifurcation Chaos Appl. Sci. Eng.* **9**, 49–65 (1999).
- ¹¹R. E. Chandler, R. Herman, and E. W. Montroll, "Traffic dynamics: Studies in car-following," *Oper. Res.* **6**, 499 (1959); D. C. Gazis, R. Herman, and R. W. Rothery, "Nonlinear follow-the-leader models of traffic flow," *ibid.* **9**, 545 (1961).
- ¹²P. S. Addison and D. J. Low, "A novel nonlinear car-following model," *Chaos* **8**, 791–799 (1998); D. J. Low and P. S. Addison, "A nonlinear temporal headway model of traffic dynamics," *Nonlinear Dyn.* **16**, 127–151 (1998).
- ¹³T. Nagatani, "Chaotic jam and phase transition in traffic flow with passing," *Phys. Rev. E* **60**, 1535–1541 (1999).
- ¹⁴M. Bando, K. Hasebe, A. Nakayama, A. Shibata, and Y. Sugiyama, "Dynamical model of traffic congestion and numerical simulation," *Phys. Rev. E* **51**, 1035–1042 (1995).
- ¹⁵S. Newhouse, D. Ruelle, and F. Takens, "Occurrence of strange axiom A attractors near quasi periodic flows on T^m , $m \geq 3$," *Commun. Math. Phys.* **64**, 35–40 (1978); D. Ruelle and F. Takens, "On the nature of turbulence," *ibid.* **20**, 167–192 (1971).
- ¹⁶E. Boe and H.-C. Chang, "Transition to chaos from a two-torus in a delayed feedback system," *Int. J. Bifurcation Chaos Appl. Sci. Eng.* **1**, 67 (1991).
- ¹⁷F. T. Arecchi, G. Giacomelli, A. Lapucci, and R. Meucci, "Dynamics of a CO₂ laser with delayed feedback," *Phys. Rev. A* **43**, 4997–5004 (1991).
- ¹⁸I. M. de la Fuente, L. Martinez, J. Veguillas, and J. M. Aguirregabiria, "Quasiperiodicity route to chaos in a biochemical system," *Biophys. J.* **71**, 2375–2379 (1996); I. M. de la Fuente, "Diversity of temporal self-organized behaviors in a biochemical system," *BioSystems* **50**, 83–97 (1999).
- ¹⁹E. Tomer, L. Safonov, and S. Havlin, "Presence of many stable nonhomogeneous states in an inertial car-following model," *Phys. Rev. Lett.* **84**, 382–385 (2000).
- ²⁰E. Tomer, L. Safonov, and S. Havlin, "Stable and metastable states in congested traffic," in *Traffic and Granular Flow '99: Social, Traffic, and Granular Dynamics*, edited by D. Helbing, H. J. Herrmann, M. Schreckenberg, and D. E. Wolf (Springer, Heidelberg, 2000), pp. 419–424.
- ²¹L. A. Safonov, E. Tomer, V. V. Strygin, and S. Havlin, "Periodic solutions of a nonlinear traffic model," *Physica A* **285**, 147–155 (2000).
- ²²S.-N. Chow and J. Mallet-Paret, "Integral averaging and Hopf bifurcation," *J. Diff. Eqns.* **26**, 112 (1977).
- ²³J. M. Franke and H. W. Stech, "Extensions of an algorithm for the analysis of nongeneric Hopf bifurcations, with applications to delay-difference equations," in *Delay Differential Equations and Dynamical Systems*, ed-

- ited by S. Busenberg and M. Martelli, *Lect. Notes in Math.* 1475 (Springer, Berlin, 1991), pp. 161–175.
- ²⁴B. D. Hassard, N. D. Kazarinoff, and Y.-H. Wan, *Theory and Applications of Hopf Bifurcation* (Cambridge University Press, Cambridge, 1981).
- ²⁵S. A. Campbell and J. Bélair, “Analytical and symbolically-assisted investigation of Hopf bifurcations in delay-differential equations,” *Can. Appl. Math. Quart. J. Dyn. Diff. Eqns.* **3**, 137–154 (1995); S. A. Campbell, J. Bélair, T. Ohira, and J. Milton, “Limit cycles, tori, and complex dynamics in a second-order differential equation with delayed negative feedback,” *J. Dyn. Diff. Eq.* **7**, 213–236 (1995).
- ²⁶E. Ya. Zhuravleva and V. V. Strygin, “Note on the small self-oscillations of systems of differential equations,” *J. Appl. Math. Mech.* **39**, 346 (1975).
- ²⁷The right-hand side of (1) can be smoothed by replacing the last term with for example $-kZ^2(v_n - v_{per})$. In this case $S(\rho)$ becomes continuous.
- ²⁸J. K. Hale, *Theory of Functional Differential Equations* (Springer, New York, 1977).
- ²⁹I. G. Malkin, *Some Problems of Theory of Nonlinear Oscillations* (U.S. Atomic Energy Commission, Washington, D.C., 1959).
- ³⁰H. G. Schuster, *Deterministic Chaos: An Introduction* (VCH, Weinheim, 1995).
- ³¹C. J. G. Evertsz and B. B. Mandelbrot, “Multifractal measures,” in *Chaos and Fractals: New Frontier of Science*, edited by H.-O. Peitgen, H. Jürgen, and D. Saupe (Springer-Verlag, New York, 1992), pp. 921–953.
- ³²T. C. Halsey, M. H. Jensen, L. P. Kadanoff, I. Procaccia, and B. I. Shairman, “Fractal measures and their singularities: The characterization of strange sets,” *Phys. Rev. A* **33**, 1141–1151 (1986).
- ³³P. Grassberger and I. Procaccia, “Measuring the strangeness of strange attractors,” *Physica D* **9**, 189–208 (1983); K. Pawelzik and H. G. Schuster, “Generalized dimensions and entropies from a measured time series,” *Phys. Rev. A* **35**, 481–484 (1987).
- ³⁴Y. Ashkenazy, “The use of generalized information dimension in measuring fractal dimension of time series,” *Physica A* **271**, 427–447 (1999).
- ³⁵J. L. Kaplan and J. A. Yorke, in *Functional Differential Equations and Approximations of Fixed Points*, Lecture Notes in Mathematics 730, edited by H.-O. Peitgen and H.-O. Walther (Springer-Verlag, Berlin, 1979).
- ³⁶M. T. Rosenstein, J. J. Collins, and C. J. de Luca, “A practical method for calculating largest Lyapunov exponent from small data sets,” *Physica D* **65**, 117–134 (1993) (we used the algorithm available at www.physionet.org).
- ³⁷A. Wolf, J. B. Swift, H. L. Swinney, and A. Vastano, “Determining Lyapunov exponents from a time series,” *Physica D* **16**, 285–317 (1985).